Molecular Cell
Article

Rapid Phospho-Turnover by Receptor Tyrosine Kinases Impacts Downstream Signaling and Drug Binding

Laura B. Kleiman,[1,2,4] Thomas Maiwald,[1] Holger Conzelmann,[1] Douglas A. Lauffenburger,[3] and Peter K. Sorger[1,3,*]
[1]Center for Cell Decision Processes, Department of Systems Biology, Harvard Medical School, Boston, MA 02115, USA
[2]Computational and Systems Biology
[3]Department of Biological Engineering
Massachusetts Institute of Technology, Cambridge, MA 02139, USA
[4]Present address: Molecular Pathology Unit, Center for Cancer Research, and Center for Systems Biology, Massachusetts General Hospital, Charlestown, MA 02129, USA
*Correspondence: peter_sorger@hms.harvard.edu
DOI 10.1016/j.molcel.2011.07.014

SUMMARY

Epidermal growth factor receptors (ErbB1–4) are oncogenic receptor tyrosine kinases (RTKs) that regulate diverse cellular processes. In this study, we combine measurement and mathematical modeling to quantify phospho-turnover at ErbB receptors in human cells and to determine the consequences for signaling and drug binding. We find that phosphotyrosine residues on ErbB1 have half-lives of a few seconds and therefore turn over 100–1000 times in the course of a typical immediate-early response to ligand. Rapid phospho-turnover is also observed for EGF-activated ErbB2 and ErbB3, unrelated RTKs, and multiple intracellular adaptor proteins and signaling kinases. Thus, the complexes formed on the cytoplasmic tail of active receptors and the downstream signaling kinases they control are highly dynamic and antagonized by potent phosphatases. We develop a kinetic scheme for binding of anti-ErbB1 drugs to receptors and show that rapid phospho-turnover significantly impacts their mechanisms of action.

INTRODUCTION

The epidermal growth factor receptor (ErbB1/EGFR) is a prototypical receptor tyrosine kinase (RTK) that activates multikinase phosphorylation cascades and regulates diverse cellular processes including proliferation, migration, and differentiation (Citri and Yarden, 2006). Differential binding of 13 known extracellular ligands to ErbB1–4 receptors induces formation of homo- and hetero-oligomers. In the case of ErbB1, whose structure has been studied in detail, ligand binding is thought to promote a conformational switch that positions the C-terminal cytoplasmic tail of one receptor near the activation loop of the other, thereby facilitating phosphorylation in *trans* (Zhang et al., 2006). Receptor dimers can form in the absence of ligand but the switch to an active conformation probably occurs only upon ligand binding (Chung et al., 2010). In solid tumors ErbB receptors are frequently mutated, overexpressed or activated by autocrine or paracrine ligands (Holbro and Hynes, 2004), and multiple small molecule kinase inhibitors and therapeutic antibodies targeting ErbB receptors are in clinical use (Tables S1 and S2). In many cases, the reasons for the differential effectiveness of these drugs are not well understood.

Active ErbB receptors phosphorylate each other on four to 12 tyrosine residues that serve as docking sites for recruitment of diverse adaptor proteins containing Src homology domain 2 (SH2) and phosphotyrosine binding (PTB) domains (Jones et al., 2006; Kaushansky et al., 2008; Schulze et al., 2005). Adaptors, and the proteins that bind to them, are often themselves targets for phosphorylation by ErbB receptors or by cytoplasmic kinases. This leads to assembly of large multiprotein "signalosomes" that transmit signals to downstream pathways including the Raf-MEK-ERK (MAPK) and PI3K-Akt kinase cascades (Yarden and Sliwkowski, 2001) and the actin cytoskeleton (Hirsch et al., 2006) (Figure 1A). In cells exposed to exogenous ligand, phosphorylation of receptors and adaptor proteins usually peaks within 10 min and then declines to prestimulus levels ~1–2 hr later, thereby driving the immediate-early response. Endocytosis and degradation of activated ErbB1 in the lysosome plays the primary role in receptor adaptation (Sorkin and Goh, 2009), but internalization is less important for ErbB2-4 (Baulida et al., 1996). Extensive evidence also points to a regulatory role for protein tyrosine phosphatases (PTPs) in ErbB biology (Table S3) (Tiganis, 2002), but it remains poorly understood how receptors are controlled by a combination of changes in receptor conformation, oligomerization, phosphorylation/dephosphorylation, and localization. The classical view is that conformational changes triggered by ligand binding drive the rapid formation of tyrosine phosphorylated ErbB1 (ErbB1-pY) and that the subsequent slower fall in ErbB1-pY levels involves relocalization of receptors to phosphatase-rich intracellular compartments, and attenuation of signaling via endocytic degradation and the action of transcriptional feedback loops (Avraham and Yarden, 2011). However, several experiments suggest a more

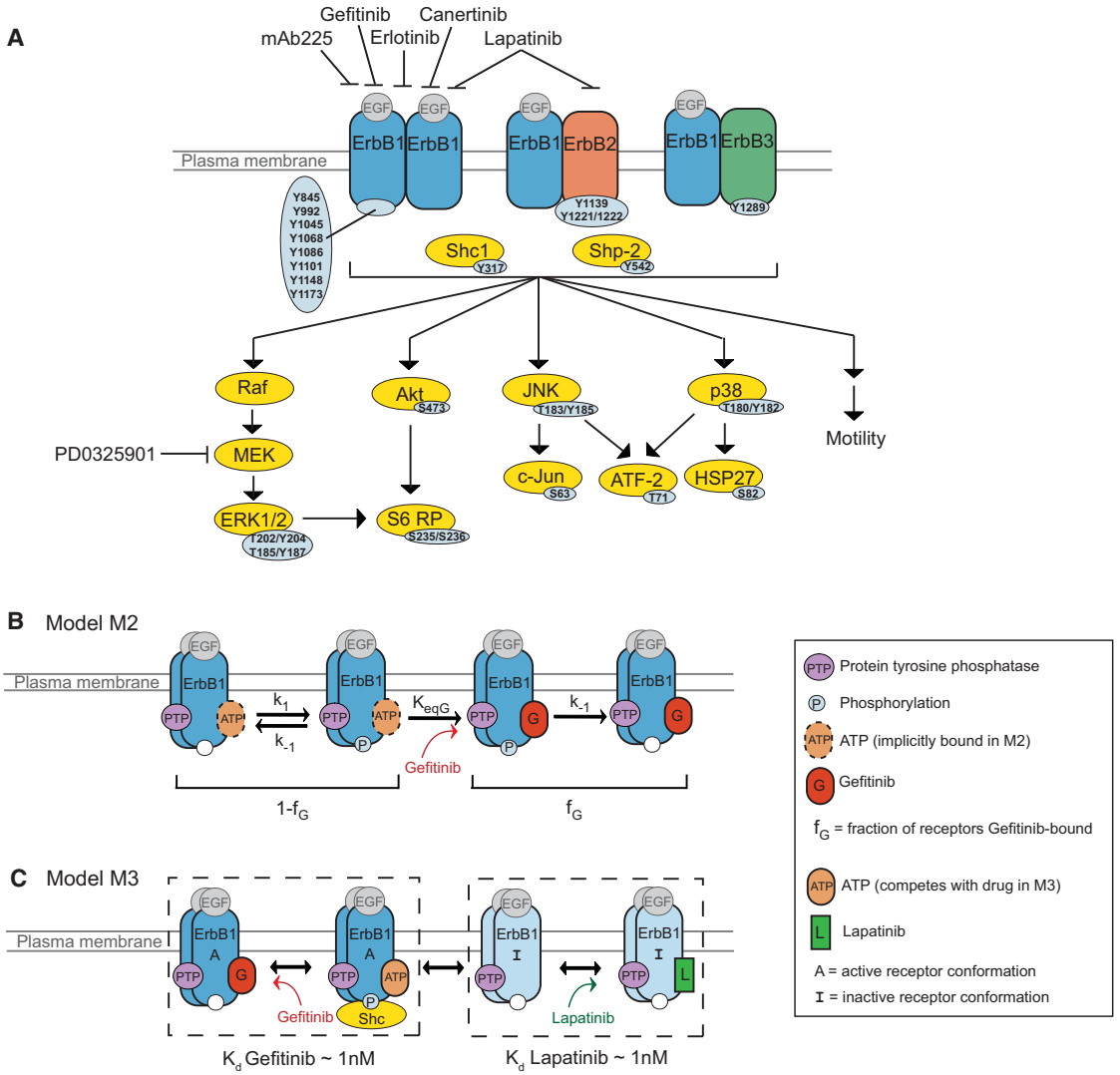

D

Model	ODEs	Parameters	Identifiable?	Key Parameters		Description
				Phos Rate	Dephos Rate	
M1	1	1	Y	---	> 7/min	Exponential decay from peak levels
M2	1	3	Y	> 4.5/min	> 8/min	Phosphorylation/dephosphorylation, gefitinib binding
M2-MC	---	---	---	mean lifetime of dephos state < 14 sec	mean lifetime of phos state < 8 sec	Stochastic model using M2 rates
M3	47	21	N	120/min	60/min	Two ErbB1 conformations, lapatinib and gefitinib binding, competition with ATP, phosphatase, Shc
M3-V1	47	21	N	(poor fit)		Only drug-bound receptors dephosphorylated
M3-V2	29	18	N	(poor fit)		Gefitinib and lapatinib only bind the active conformation
M3-V3	53	23	N	(no significant binding to active conformation)		Lapatinib binds both conformations

Figure 1. Overview of Relevant RTK Signaling and Mathematical Models

(A) Schematic of phospho-sites assayed for ErbB1–3 and downstream proteins.

(B) Model M2: A simple biochemical scheme describing ErbB1 phosphorylation, dephosphorylation, and gefitinib binding.

(C) Model M3: A more detailed biochemical scheme describing ErbB1 conformational switching, binding of gefitinib, lapatinib, Shc, and phosphatase, and competition between drug and ATP for binding to receptor.

(D) Key details and results from the various models. For model M3, parameter values for the median of 200 best fits are reported.

See also Tables S1 and S2.

dynamic balance between activation and inactivation. For example, treatment of cells with the potent pan-specific tyrosine phosphatase inhibitor pervanadate causes large and immediate increases in ErbB1-pY (and increased phosphotyrosine levels on many other proteins) in the absence of added ligand (Ruff et al., 1997), implying a requirement for phosphatases in opposing receptor autoactivation. In addition, sequential exposure of cells to ligand and then to a small molecule kinase inhibitor causes phosphorylation to rise and then fall rapidly (Böhmer et al., 1995; Offterdinger et al., 2004). These data on turnover of tyrosine phosphates on ErbB1 motivated us to perform a more quantitative and extensive study.

Here, we use a series of mathematical models (Figures 1B–1D) and detailed time course data to address five unanswered questions about RTK phosphorylation: (1) What is the rate at which tyrosine phosphorylation turns over on active ErbB1 receptors under various conditions? (2) Is the rapid dephosphorylation an artifact of drug binding? (3) Is the pool of ErbB1 subject to rapid dephosphorylation the same pool that is active in signal transduction, and, if so, what are the consequences of rapid phospho-turnover for downstream signaling? (4) Do other ErbB receptors and unrelated RTKs also exhibit rapid phospho-turnover? (5) What are the consequences of ErbB phospho-turnover for the mechanisms of action of small molecule drugs that bind ErbB receptors? The latter question seemed particularly interesting because in vitro studies on anti-ErbB drugs have been performed in the absence of phosphatases. We report that ErbB1–3, the insulin-like growth factor 1 receptor (IGF1R), and the fibroblast growth factor receptor 1 (FGFR1) cycle between phosphorylated and unphosphorylated states on the time scale of seconds and that phosphorylated forms of downstream kinases such as ERK, Akt, JNK, and p38 also turn over rapidly. We argue this is unlikely to be an artifact of drug binding. This implies that a single RTK molecule is phosphorylated and dephosphorylated at least 100–1000 times over the course of an ~1 hr immediate-early response. Rapid phosphorylation and dephosphorylation of RTKs has significant implications for signalosome assembly and mechanisms of kinase inhibition.

RESULTS

Rapid ErbB1 Dephosphorylation Regardless of Intracellular Localization

We studied ErbB receptor activation and inactivation in diverse human tumor lines including transformed H1666, HeLa and HepG2 cells and nontransformed MCF-10A cells. Serum starved cells were treated with the ErbB1 ligand EGF and receptor phosphorylation levels were then measured by using phospho-site-specific antibodies in multiple formats including immunofluorescence, western blotting and ELISA. We also used a sandwich immunoassay that does not rely on having antibodies selective for specific phosphorylation sites (the EpiQuant assay from Millipore). In the EpiQuant method, proteolytic fragments of receptor are captured on Luminex xMAP beads with peptide-specific antibodies and modifications are detected with pan-specific anti-phosphotyrosine antibodies. We obtained nearly identical results with all assays except that the signal to noise was greatest with the EpiQuant method (see the Supplemental Experimental Procedures for details). In H1666 cells, levels of ErbB1-pY1173 (a binding site for the Shc adaptor protein) (Jones et al., 2006) increased 5- to 10-fold within 10 min of EGF addition and then fell with a half-life ($t_{1/2}$) of ~30 min, returning to prestimulus levels by 2 hr, concomitant with a fall in surface and total ErbB1 (Figure 2A and Figure S1A). However, when cells were first stimulated with EGF and the clinical-grade ErbB1 kinase inhibitor gefitinib (Karaman et al., 2008) was added 10 min later, ErbB1-pY1173 levels declined exponentially to near basal levels with $t_{1/2}$ ~15 s (Figure 2B, red curve). No decrease in total ErbB1 was observed (Figure 2C), consistent with the fact that gefitinib blocks receptor internalization and degradation (Nishimura et al., 2007). ErbB1 must therefore be dephosphorylated rather than degraded. Rapid ErbB1 dephosphorylation was observed for all eight tyrosine residues on the ErbB1 tail for which we could establish reliable assays (Figure 2D and Figure S1B) as well as after exposure of cells to different doses of EGF (Figure S1C) or to other ErbB1 ligands (e.g., amphiregulin; data not shown). While H1666 cells express only wild-type ErbB1, rapid dephosphorylation of ErbB1 was also observed in tumor cell lines that carry oncogenic, gefitinib-sensitizing mutations (e.g., H3255 cells; data not shown) (Paez et al., 2004), demonstrating that it is not unique to wild-type receptor. Finally, ErbB1 was rapidly dephosphorylated after treatment of cells with the ErbB1 ATP-competitive kinase inhibitor erlotinib (data not shown) and with canertinib (CI-1033; Figure 2B, orange curve), a structurally different drug that covalently modifies the kinase active site. From these data, we conclude that rapid ErbB1 dephosphorylation occurs at multiple phosphotyrosine residues, under a wide variety of conditions and in the presence of kinase inhibitors differing in chemical structures and mechanisms of action.

The best-characterized PTP for ErbB1, PTP1B, resides in the endoplasmic reticulum (ER) and interacts with receptors in perinuclear ER compartments ~30 min after EGF stimulation (Haj et al., 2002). We therefore asked whether ErbB1 had to translocate to the ER for efficient dephosphorylation. In EGF-stimulated cells ErbB1 was found largely on the plasma membrane at t = 2 min, in early endosomes by t = 10 min, and in late perinuclear endosomes by t = 30 min (Figure S1D). Receptor localization was not observably altered by 1 min of gefitinib exposure at t = 10 min (Figure S1D) and ErbB1-pY1173 turned over with $t_{1/2}$ ~15 s regardless of the interval between EGF and gefitinib addition in a 2–30 min window (Figure 2E). We conclude that ErbB1 is dephosphorylated rapidly following drug addition regardless of cellular localization and thus, that receptors are continuously accessible to potent PTPs.

Rapidly Dephosphorylated RTKs Are Active in Signaling

It is possible that only a subset of phosphorylated ErbB1 is actively involved in signaling to downstream kinases and that the pool of ErbB1 subject to rapid dephosphorylation is not the relevant population for signal transduction. We therefore asked whether rapid inactivation of EGF-stimulated ErbB1 by gefitinib would propagate to receptors such as ErbB2 and ErbB3 that are phosphorylated by ErbB1 in *trans* and also to cytosolic kinases that transduce signals downstream of ErbB1 such as ERK, Akt, JNK, and p38. In H1666 cells, we observed both

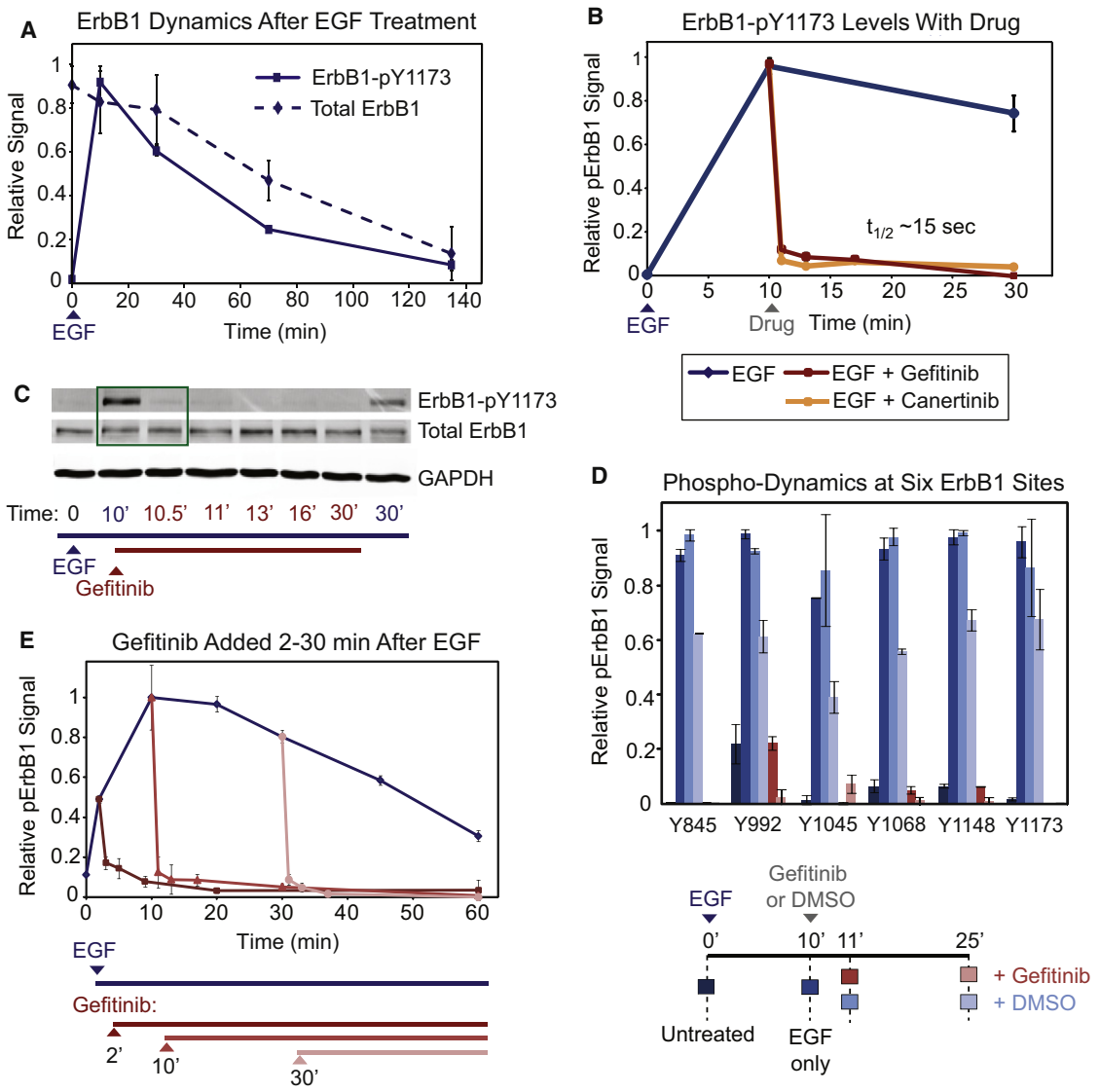

Figure 2. ErbB1 Is Rapidly Dephosphorylated after Gefitinib Treatment

High-throughput fluorescence microscopy (HTM) measurements of total ErbB1 (cell surface plus internal) or ErbB1-pY1173 after "activation-inhibition" experiments where serum starved H1666 cells were stimulated with 100 ng/ml EGF followed by addition of 10 μM gefitinib or canertinib 10 min later (unless otherwise noted). Pooled data are represented as mean ± standard deviation (SD) and normalized between 0 and 1.

(A) Receptor dynamics following EGF treatment. The two time courses were normalized separately and are not directly comparable.

(B–D) Activation-inhibition experiments as measured by HTM (B), western blotting (C), or ELISA (D). In (D), cells were treated with EGF for 10 min and gefitinib or a DMSO control was then added for 1 or 15 additional min.

(E) Activation-inhibition experiment with gefitinib added 2, 10, or 30 min after EGF.

See also Figure S1.

ErbB2-Y1221/1222 (a Shc binding site) and ErbB3-Y1289 (a PI3K binding site) (Schulze et al., 2005) to be phosphorylated 10 min after EGF exposure and then rapidly dephosphorylated upon subsequent addition of gefitinib ($t_{1/2}$ ~15 s and 32 s, respectively; Figure 3A). Shc1 was ErbB1-bound and phosphorylated following EGF addition but upon subsequent addition of gefitinib, Shc1-pY317 was rapidly dephosphorylated ($t_{1/2}$ ~26 s) and Shc1 dissociated from receptors ($t_{1/2}$ ~14 s; Figure 3B and Figure S2). These phenomena do not appear to be cell-type specific: when ErbB1 and ErbB2 were assayed in MCF-10A, HeLa and HepG2 cells we observed phospho-receptor half-lives after gefitinib exposure to be ~10–15 s in all cases (Figures 3C and 3D). No correlation was observed between natural rates of receptor inactivation, which varied from $t_{1/2}$ ~10 min in HeLa cells to ~90 min in HepG2 cells, and the rate of phospho-turnover after gefitinib addition, which was always fast. Net receptor levels in the absence of drug are presumably set by a dynamic balance between ligand binding/unbinding,

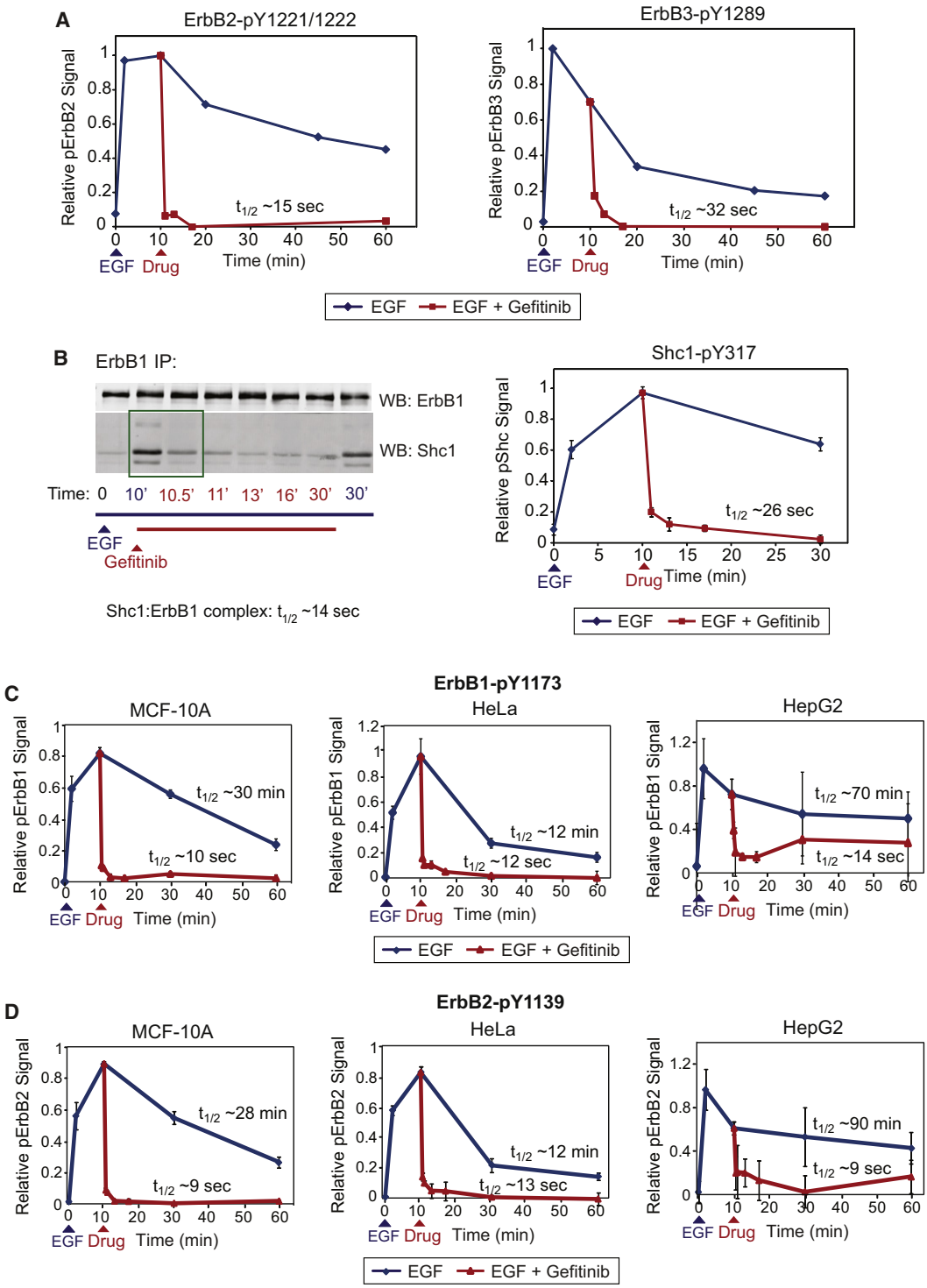

Figure 3. ErbB1 and Its Binding Partners Experience Rapid Phospho-Turnover across Cell Lines

(A) ErbB2 and ErbB3 phosphorylation measured by ELISA in H1666 cells in activation-inhibition experiments.

(B) Coimmunoprecipitation of ErbB1 and Shc1 in H1666 cells (left) and HTM measurements of Shc1 phosphorylation (right). The three Shc1 bands on the western blot correspond to different isoforms.

(C and D) Reverse phase protein lysate array (RPPA) measurements of ErbB1 (C) and ErbB2 (D) phosphorylation in activation-inhibition experiments in three additional cell lines.

See also Figure S2.

phosphorylation/dephosphorylation and trafficking to and from the plasma membrane.

The Akt and MAPK pathways are two critical kinase cascades downstream of ErbB receptors. In both MCF-10A and H1666 cells, levels of Akt-pS473 increased after EGF exposure and then fell rapidly upon subsequent addition of gefitinib ($t_{1/2}$ ~100 and ~60 s; Figure 4A). The same was true of ERK1/2-pT202/Y204 in MCF-10A cells ($t_{1/2}$ ~210 s; Figure 4B, left). Moreover, lamellipod extension, an immediate-early EGF response involved in cell migration (Segall et al., 1996), was also inhibited within 40 s of gefitinib addition (Figures S3A–S3C). We conclude that the pool of ErbB1 receptors subject to rapid dephosphorylation is the pool active in signaling to physiologically important downstream processes and that Akt, ERK and lamellipod extension are themselves targets of potent negative regulation by phosphatases (either directly or indirectly).

In EGF-treated H1666 cells, ERK dephosphorylation was substantially slower after gefitinib treatment ($t_{1/2}$ > 10 min; Figure 4B, right, and Figure S3D) than in MCF-10A cells, implying either that ERK phosphatases are not as active as in MCF-10A cells or that the activating signal sent by ErbB1 is longer lived. To distinguish between these possibilities, EGF-stimulated H1666 cells were treated with PD0325901, a non-ATP competitive MEK inhibitor that locks the enzyme in a catalytically inactive conformation. PD0325901 exposure resulted in rapid ERK dephosphorylation ($t_{1/2}$ ~40 s; Figure 4B, right) arguing that potent ERK phosphatases are present in H1666 cells but that, in the absence of phosphorylated receptor, proteins downstream of ErbB1 and upstream of ERK remain active for longer than in MCF-10A cells. Raf kinase is mutated in H1666 (Pratilas et al., 2008) but not MCF-10A cells and may be responsible for prolonging ERK signaling in the former. When nine EGF-activated signaling proteins including receptor adaptors, kinases, and transcription factors were examined in four cell lines we consistently observed significantly more rapid dephosphorylation in the presence of gefitinib than in its absence; for example, Akt-pS473 had a $t_{1/2}$ ~4–120 min in the absence of gefitinib and $t_{1/2}$ ~40–130 s in its presence (heat maps are shown in Figure 4C and time course data in Figure S3E). However, we also observed that some EGF-induced modifications (S6-pS235/236 for example) lasted long after receptors were inactivated. This reflects the absence of potent S6 phosphatases in cells or a decoupling between upstream and downstream signals (as observed with ERK in H1666 cells) and points to an aspect of signal transduction dynamics that has not previously been studied.

The fact that multiple proteins activated by ErbB1 are subject to as rapid dephosphorylation as ErbB1 after gefitinib addition demonstrates that high phospho-turnover is not restricted to drug-bound receptors. It is therefore difficult to argue that the phenomenon is an artifact of drug binding. However, as a second means to inactivate receptors we allowed ligand to dissociate while blocking rebinding with the anti-ErbB1 receptor monoclonal antibody mAb225. With amphiregulin, a low-affinity ErbB1 ligand that has a fast off rate (Neelam et al., 1998; Roepstorff et al., 2009), ErbB1-pY1173 levels decayed exponentially with $t_{1/2}$ ~2 min (and with EGF, $t_{1/2}$ ~10 min; Figure 5A). These rates are substantially faster than the normal (net) rate of receptor dephosphorylation ($t_{1/2}$ > 1 hr for amphiregulin and ~30 min for EGF in H1666 cells), arguing that in the absence of drugs ErbB1 is rapidly inactivated by phosphatases when ligand dissociates.

Finally, we asked whether RTKs other than ErbB receptors exhibit rapid phospho-turnover. In MCF-10A cells stimulated with IGF1 for 10 min we observed an increase in IGF1R-pY1131 and Akt-pS473 and a gradual decay subsequently. However, when cells were treated with the IGF1R-selective kinase inhibitor NVP-AEW541, both IGF1R and Akt were rapidly dephosphorylated ($t_{1/2}$ ~80 s and 130 s, respectively; Figure 5B). Akt-pS473 also fell rapidly following addition of FGF1 and then the FGFR1-specific drug PD173074 (Figure S4; phospho-FGFR1 levels could not be reliably measured). These data suggest that rapid phospho-turnover may be a general feature of RTKs.

Quantifying ErbB1 Phospho-Turnover with Kinetic Models

To explore the consequences of rapid phospho-turnover for ErbB1 biochemistry we need models that can be compared rigorously to data. Receptors and immediate-early signaling molecules are relatively abundant and we therefore used mass action kinetics as represented by networks of compartmentalized, ordinary differential equations (ODEs). By incorporating data from in vitro studies and calibrating models against time course data from cells we were able to estimate rates of ErbB1 phosphorylation and dephosphorylation under different conditions (calibration in this context refers to repeated rounds of fitting the model against experimental data while recording the range of parameter values that return a good fit; see the Supplemental Experimental Procedures, Computational Procedures S2 and S4 for details). More importantly, we could instantiate different biochemical schemes in models and rigorously determine which ones best represent the data.

In modeling ErbB receptors we must choose between simple models that are not particularly realistic but for which available data tightly constrain rate constants and uncertainty arises only from experimental error (making the models identifiable), and more complex and realistic models that are non-identifiable. To balance the competing demands of biological realism and model identifiability, we constructed a series of models of increasing complexity (M1–M3; Figures 1B–1D), guided by the principle that for any specific set of data, the simplest model compliant with the measurements is generally the best. The least complex "model" (M1) lacks mechanistic detail and assumes exponential decay from peak phospho-ErbB1 levels at t = 10 min; the phosphorylation half-lives reported above were calculated using this model. M1 yielded a net ErbB1-pY1173 dephosphorylation rate constant of ~0.02/min in cells treated with EGF alone and ~7/min in cells subsequently exposed to gefitinib. Using measured values of ~10^5 ErbB1 molecules per H1666 cell and maximal fractional phosphorylation of 0.4 (see the Supplemental Experimental Procedures, Computational Procedure S1 for details), we computed that approximately ten net receptors are dephosphorylated per cell per second with EGF alone (at t = 10 min) versus 5 × 10^3 after gefitinib treatment. Conversely, maintenance of high net levels of ErbB1 phosphorylation in the absence of gefitinib requires rapid receptor rephosphorylation.

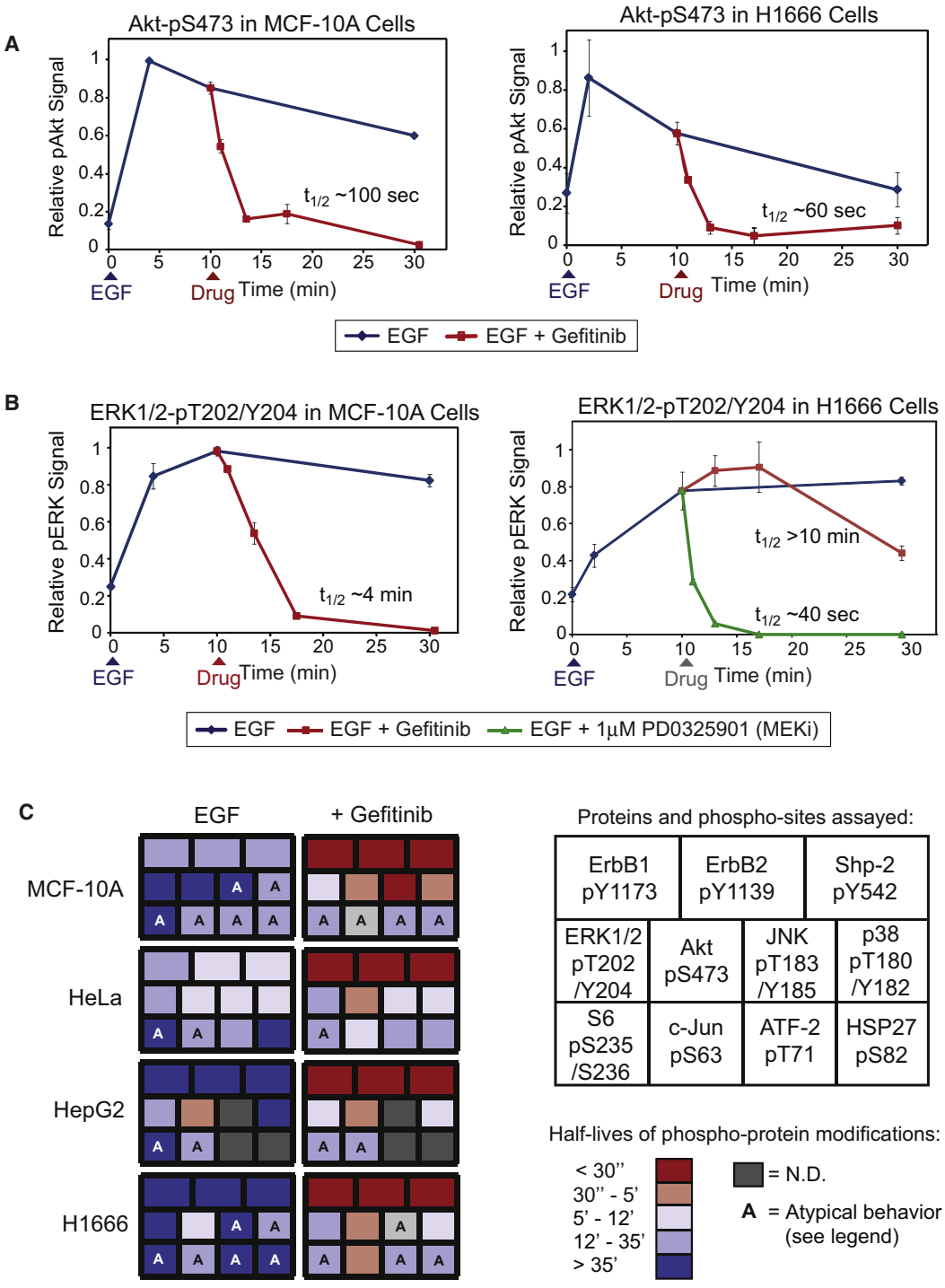

Figure 4. Downstream Proteins Also Exhibit Rapid Phospho-Dynamics

(A and B) HTM measurements of Akt (A) and ERK (B) phosphorylation after treatment of MCF-1A and H1666 cells with EGF and then 10 μM gefitinib or 1 μM PD0325901, a MEK inhibitor

(C) Heat map of approximate half-lives (calculated from t = 10 min) for dephosphorylation of various proteins as measured by RPPA in activation-inhibition experiments with 10 μM gefitinib added 10 min after EGF in four cell lines. Atypical means that phosphorylation levels rose after 10 min of EGF exposure and the maximum was not reached by the time of drug addition: light gray, protein not phosphorylated by 10 min EGF and no change in phospho-signal with gefitinib; dark blue, no decline in phospho-signal over the time measured; light blue, late decline. N.D. (dark gray) indicates that the signal was not detected.

See also Figure S3.

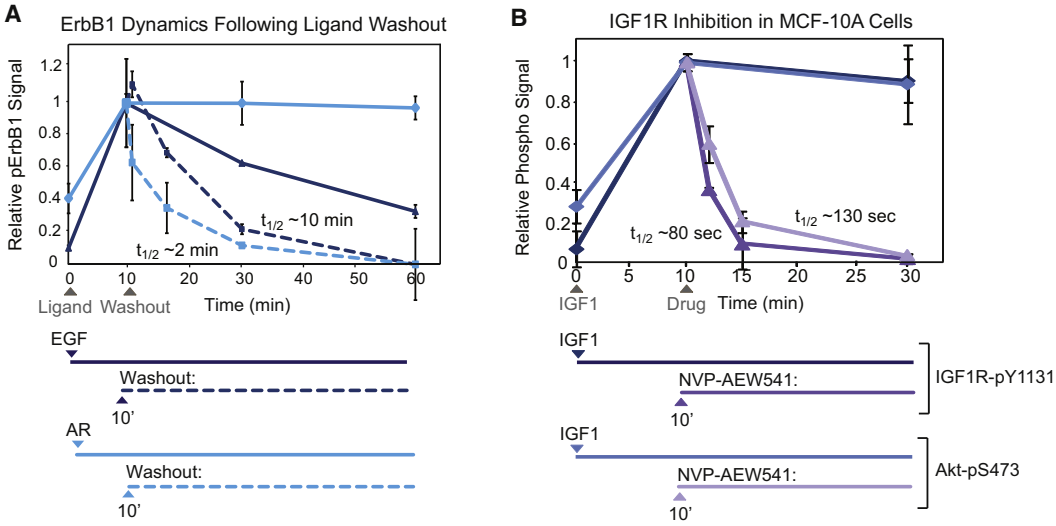

Figure 5. Activation-Inhibition Experiments with Ligand Washout and an IGF1R-Specific Inhibitor

(A) HTM measurements of ErbB1-pY1173 in H1666 cells. After 10 min exposure to 100 ng/ml EGF or 177 ng/ml amphiregulin (AR) (both 16 nM), ligand was removed and replaced with conditioned media plus mAb225.

(B) IGF1R-Y1131 and Akt-S473 dephosphorylation as measured by western blotting in MCF-10A cells after 100 ng/ml IGF1 stimulation followed by addition of 20 μM NVP-AEW541 (an IGF1R-specific kinase inhibitor). Quantification was performed by background subtraction and normalization to GAPDH.

See also Figure S4.

The simplest biochemical scheme for ErbB1-gefitinib interaction (model M2) encompasses receptors cycling between unmodified and modified (phosphorylated) states, both of which can be bound by drug (Figure 1B; see the Supplemental Experimental Procedures, Computational Procedure S2 for details). M2 involves a separation of time scales that focuses on the 10 min period after gefitinib addition and ignores initial receptor activation prior to drug exposure as well as slower processes such as receptor degradation. Because ErbB1 is expressed at much higher levels than ErbB2-4 in H1666 cells (Supplemental Experimental Procedures), M2 includes only ErbB1. Binding of gefitinib to ErbB1 is assumed to be independent of receptor phosphorylation and in quasi-equilibrium, a reasonable assumption since drug-receptor interactions are likely diffusion limited (Northrup and Erickson, 1992). Gefitinib binds and inactivates receptors by displacing ATP, which is present implicitly. It can be shown analytically that M2 is identifiable for the phosphorylation and dephosphorylation rate constants (k_1 and k_{-1}, respectively) and for the apparent association constant for gefitinib binding (K_{eqG}).

To calibrate model M2 we collected a detailed dataset in which ErbB1-pY1173 levels were measured with a high sampling rate in H1666 cells exposed to EGF and subsequently to 1–20 μM gefitinib at t = 10 min (Figure 6A). At 10–20 μM gefitinib, ErbB1-pY1173 exhibited $t_{1/2}$ ~5 s and near-complete receptor dephosphorylation within 20 s, as described above. However, when gefitinib was added at 1 μM results were qualitatively different: ErbB1-pY1173 levels fell rapidly at first but then plateaued at ~50% of initial levels. When M2 was calibrated against data from cells treated with 1 or 10 μM gefitinib it accurately predicted the effects of exposure to 5 or 20 μM gefitinib (Figure S5A; rmsd = 0.04). Calibration across all data yielded k_1 ~4.5/min ($\sigma = 1.6$), k_{-1} ~8/min ($\sigma = 0.7$) and K_{eqG} ~1.3 μM^{-1} ($\sigma = 0.9$) (Figure 6B). These numbers are consistent with in vitro estimates for k_1, which range from ~1.5/min to ~20/min (Qiu et al., 2009; Yun et al., 2008). Our estimate for K_{eqG} reflects competition with intracellular ATP and the Cheng-Prusoff equation yields a K_d ~2.5 nM, close to the in-vitro value of ~1 nM (Karaman et al., 2008). Thus, rate constants estimated for M2 fit well with previous data obtained from detailed in vitro studies implying that M2, for all its simplifications, is a reasonable representation of ErbB1-Y1173 phospho-dynamics. By assuming phosphorylation/dephosphorylation events to be Poisson-like processes and performing Monte Carlo-based simulations, we estimate the mean lifetime of unmodified ErbB1 in the presence of EGF to be ~14 s and the phospho-state to be ~8 s (model M2-MC; Figures S5B and S5C; see the Supplemental Experimental Procedures, Computational Procedure S3 for details). The mean lifetime of the unmodified state increases to ~30 s with 1 μM gefitinib present and ~190 s with 10 μM gefitinib.

Model M3: A Model for Comparing Gefitinib and Lapatinib

The data described above pertain to drugs such as gefitinib that are thought to bind to ErbB1 in an active conformation. However, a second class of drugs has been developed that binds to inactive receptors. In the case of lapatinib, a drug of this class that has been successful as a clinical agent, tight binding is also observed to ErbB2 (K_d ~5 nM for both receptors (Karaman et al., 2008; Wood et al., 2004). When we compared ErbB1-pY1173 phospho-dynamics in EGF-treated cells exposed to gefitinib or lapatinib, we observed two significant differences. First, after exposure to lapatinib at or below the IC_{50} concentration (~1 μM) phospho-ErbB1 levels fell significantly slower than with gefitinib ($t_{1/2}$ ~8 min versus 5 s with gefitinib), but complete

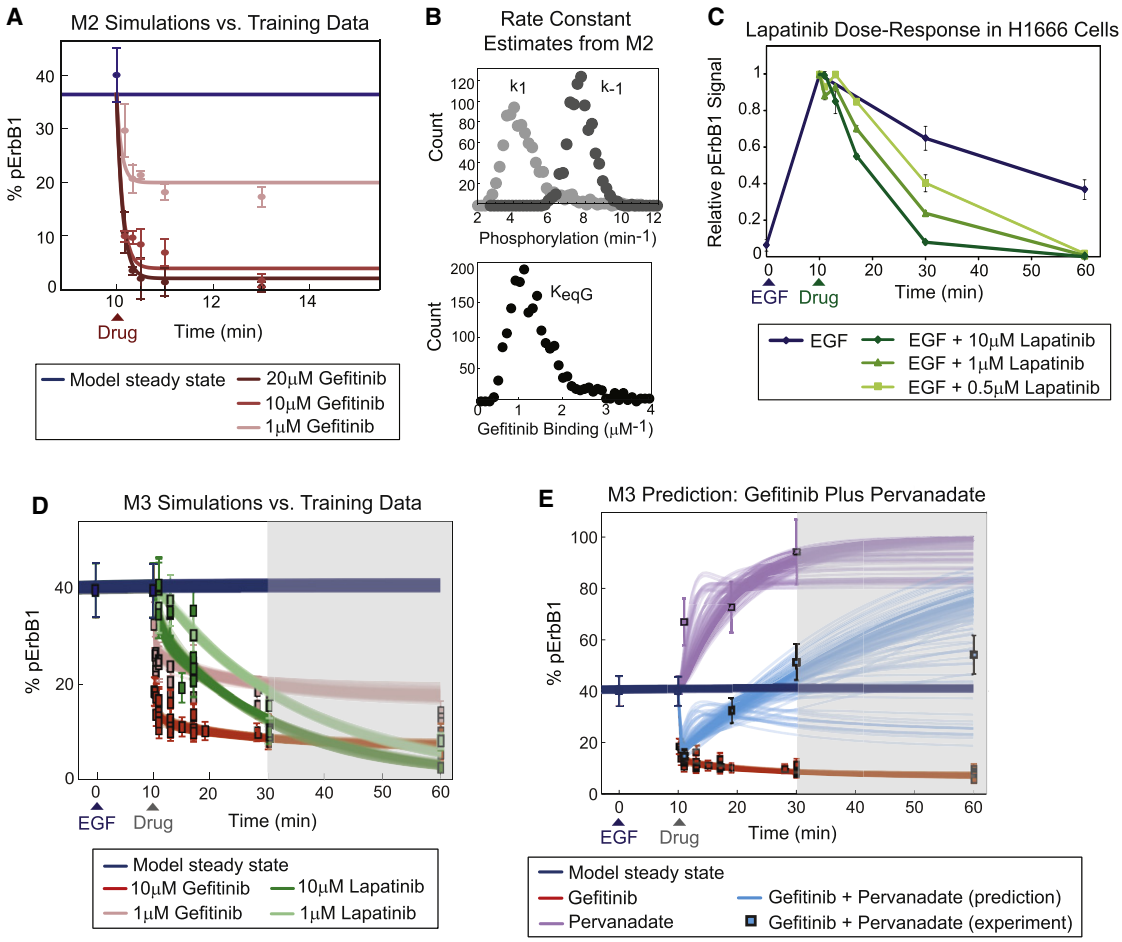

Figure 6. Model M2 Provides Estimates for Rate Constants and Model M3 Allows for Analysis of Phospho-Dynamics after Drug Treatment

ErbB1-pY1173 in H1666 cells was measured in activation-inhibition experiments by HTM.

(A) Dose-response with gefitinib (circles). M2 simulations using the median of the estimated parameter values are shown as solid curves.

(B) Estimates for kinetic parameters using a Monte Carlo simulation based on fitting with 10^3 randomly selected data values within the experimentally determined range.

(C) Dose-response with lapatinib.

(D) M3-based simulations (the best 100 model fits are shown as overlapping lines) and experimental data (individual data points, squares, are averages of replicate measurements made on the same day and error bars were calculated using an error model). The t = 0 data point was added to force model pre-equilibration; the model steady state is representative of EGF treatment alone and model assumptions begin to break down after 30 min (gray).

(E) Simulations (lines) and experimental data (squares) for individual or combination treatment with 10 μM gefitinib and 100 μM pervanadate. Data for the individual treatments were used during fitting whereas the combination was not.

Data in (A), (D) and (E) were normalized as described in the Supplemental Experimental Procedures, Computational Procedure S4. See also Figure S5.

inhibition was observed by 60 min regardless of dose (Figure 6C). In contrast, treatment of cells with gefitinib near that drug's IC_{50} value (also ~1 μM) resulted in rapid but partial receptor inhibition (Figures 6A and 6D).

To compare lapatinib and gefitinib we created model M3, representing a consensus view of drug mechanism of action, as well as a series of variant models (M3-V1, V2, and V3) that explored alternative biochemical hypotheses (see the Supplemental Experimental Procedures, Computational Procedure S4 for details). The parental M3 model includes a switch between active and inactive ErbB1 conformations, stronger binding of ATP and gefitinib to active ErbB1, and preferential binding of lapatinib to inactive ErbB1 in a manner that blocks the transition to an active conformation (Johnson, 2009; Wood et al., 2004) (Figure 1C). Finally, we assumed phosphatases to associate reversibly with receptors and Shc to bind reversibly to ErbB1-pY1173, protecting phosphotyrosine residues from phosphatases when bound. Because the relative affinities of ATP and gefitinib for active versus inactive ErbB1 are unknown, they were considered as adjustable parameters whose values were estimated by calibration. Implementing these assumptions, with other details similar to those of M2, resulted in a model with 47 ODEs and 21 parameters. Data for M3 calibration consisted of 12 sets of ErbB1-pY1173 dynamics in cells treated first with EGF for 10 min and then with 0.25–20 μM gefitinib or 0.5–10 μM lapatinib (a subset of the data is shown in Figure 6D and the entire data set is

provided in the Supplemental Information). To aid calibration, some parameters were constrained within ranges consistent with in vitro observations. M3 is expected to return faster rate constants for ErbB1 phosphorylation and dephosphorylation than M2 because drug and ATP compete for receptor binding and phosphatases compete with adaptor proteins for interaction with phosphotyrosines. Indeed, estimated rate constants were >10-fold higher in M3 than M2 (Figure 1D and Figure S5D).

M3 shows receptors to undergo at least 150 phosphorylation/dephosphorylation cycles per hour with saturating EGF and 30 cycles per hour with saturating gefitinib. Thus, treating cells with 10 μM gefitinib plus pervanadate, a pan-specific PTP inhibitor that irreversibly oxidizes a catalytic cysteine (Huyer et al., 1997), should cause an initial drop in ErbB1-pY due to rapid gefitinib binding and then a steady rise as drug dissociates and receptors become phosphorylated. This is precisely what we observed in cells (Figure 6E, cyan curves and squares). When cells were exposed to pervanadate in the absence of EGF and gefitinib, ErbB1-pY also rose to high levels (Figure S5E) (Amanchy et al., 2005). To determine whether this involved an autocrine ligand (or residual ligand from media) cells were treated with saturating mAb225 anti-ErbB1 antibody for 2 hr prior to pervanadate exposure, with no observable reduction in ErbB1-pY accumulation (Figure S5E). These data confirm model-based predictions, suggesting that even receptors lacking bound ligand are rapidly phosphorylated in the presence of gefitinib and absence of antagonizing phosphatases.

A Kinetic Scheme for ErbB1 Binding to Small Molecule Drugs

With M3 we sought to move beyond an analysis of rate constants and investigate mechanisms of drug-receptor interaction. This necessitated estimates for rates of interconversion among different drug-receptor complexes (a measure of reaction fluxes) which in turn required the development of a new in silico labeling method for calculating fluxes from calibrated, nonidentifiable ODE networks (T.M., unpublished data). With these methods in hand we asked why exposure of cells to lapatinib results in much slower ErbB1 dephosphorylation than exposure to gefitinib. Analysis of M3 by in silico labeling showed initial ErbB1 phospho-dynamics in the presence of 10 μM lapatinib to be determined by the relatively slow conversion of receptor to an inactive conformation (Figure 7A): it took ~20 min for active receptors to switch to the inactive conformation, and receptors subsequently bound lapatinib in ~30 s (these "transition times" represent the time required for 50% of receptors to switch from one state to another at least once). In contrast, initial phospho-dynamics in the presence of gefitinib were determined by fast binding of drug to the active conformation and rapid dephosphorylation (~11 s). Thus, while our model is consistent with in vitro data showing that lapatinib binds more slowly to ErbB1 than gefitinib (the on-rate for binding of gefitinib to the active ErbB1 conformation was ~12 nM/min and the on-rate for lapatinib binding to the inactive conformation was ~1.5×10^{-4} nM/min), the rate-limiting step in cells for ErbB1 dephosphorylation in the presence of lapatinib is an active-to-inactive conformational transition that is one to two orders of magnitude slower than drug binding.

Why does exposure to low-dose lapatinib result in complete receptor inhibition but low-dose gefitinib does not? From M3 we estimate that ATP binds ~5×10^4-fold less strongly to inactive than active ErbB1, consistent with a difference in the shape of the catalytic pocket (Johnson, 2009). Consequently, drugs such as lapatinib that associate with the inactive conformation encounter much less competition from intracellular ATP than drugs such as gefitinib. Moreover, M3 predicts very slow unbinding of lapatinib (~20 hr), essentially locking the receptor in the inactive state (Figure 7A). In contrast, low-dose gefitinib incompletely inhibits ErbB1 because the forward rate of phosphorylation by drug-free receptors is approximately balanced by a reverse reaction in which drug-free and drug-bound receptors are dephosphorylated. Thus, incomplete inhibition reflects the fact that active receptors continually reform, in accordance with results obtained from pervanadate treatment (Figure 6E). Simulations provided a further insight: differences between gefitinib and lapatinib can only be explained if ErbB1 phospho-turnover is rapid. If the rate of turnover is steadily decreased while fixing the ratio of the phosphorylation and dephosphorylation rate constants, gefitinib and lapatinib become more and more similar in their effects until they are indistinguishable ~20-fold below their nominal values at ~2.5/min (Figure 7B).

Inspection of our kinetic scheme reveals a number of unexpected features. For example, M3 predicts the transition time from inactive to active ErbB1 (dashed box in Figure 7A) to be ~70 min in the presence of gefitinib and >10 days in the presence of lapatinib. Since neither form of ErbB1 is drug-bound, this result seems paradoxical. However, fluxes between states are functions not only of rate constants, but also of reactant concentrations: at the quasi-steady state achieved ~3 hr after exposure to drug, the concentration of inactive and unbound ErbB1 is much lower in the presence of lapatinib than gefitinib (0.03% versus 1% of total receptors), even though the rate constant for conversion to the active conformation is the same. Thus, relative concentrations explain the long time required for transition of receptors to an active conformation when lapatinib is present. Gefitinib is generally assumed to primarily bind and inhibit an active ErbB1 conformation (Yun et al., 2007). Consistent with this, M3 predicts that gefitinib binds to active ErbB1 ~150-fold more avidly than to the inactive conformation (K_d ~1 nM versus 165 nM). Nonetheless, simulation shows that complexes between gefitinib and inactive ErbB1 are ~4-fold more abundant than complexes between gefitinib and active ErbB1 (at 10 μM gefitinib; Figure 7C). How can this be? Analysis of M3 suggests that it arises because competition between micromolar drug and millimolar intracellular ATP dominates the distribution of drug-receptor complexes. Much less competition from ATP for binding to inactive receptor conformations permits significant gefitinib association in the face of a high binding constant. If this hypothesis can be confirmed for other receptors, then it has clear implications for the design of high potency drugs.

Testing Variant Models and Model Predictions

The strength of our conclusions necessarily depends on the accuracy of hypotheses made during model construction, including the assumptions that receptors not bound to drug

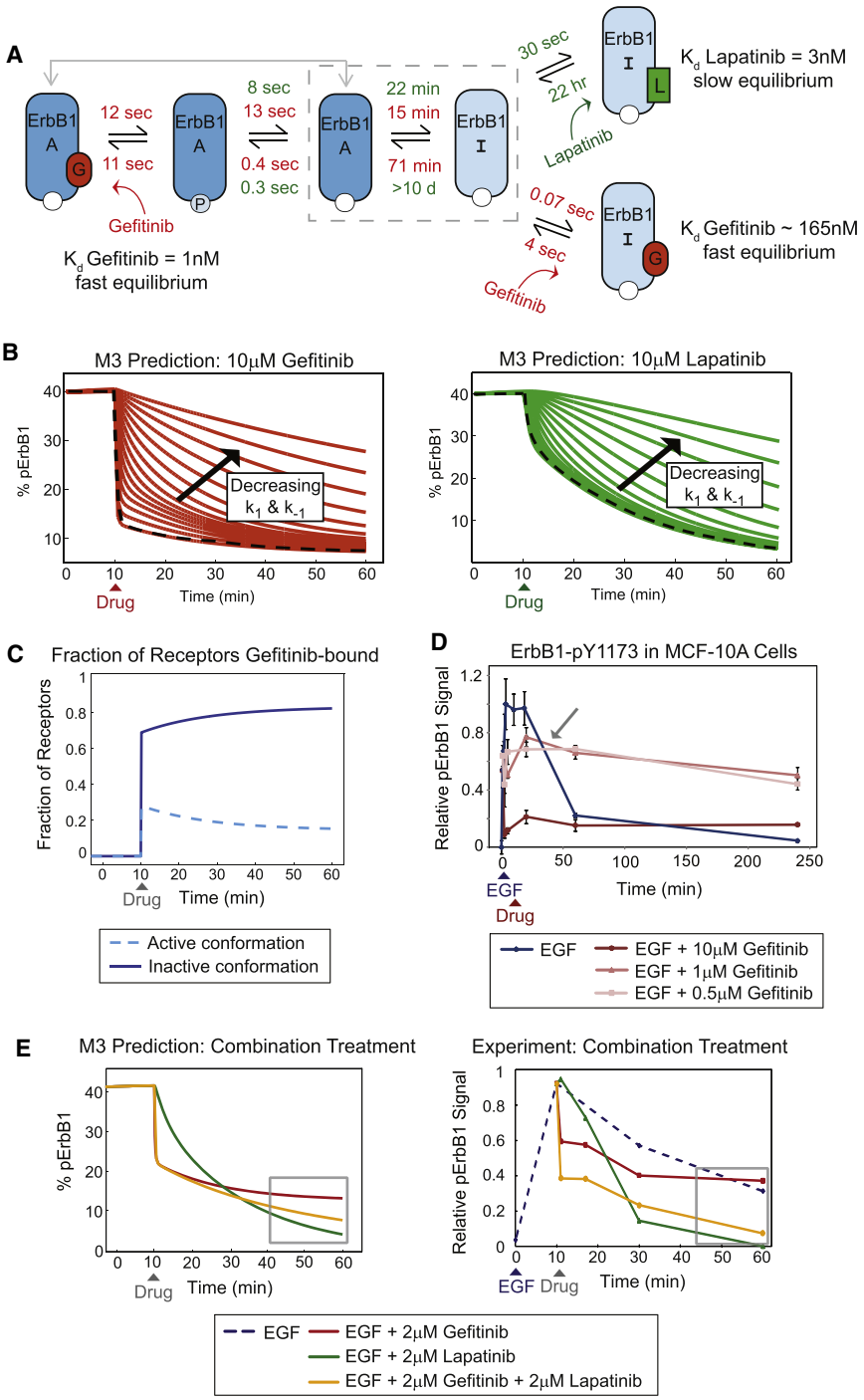

Figure 7. A Kinetic Scheme for Comparing Gefitinib and Lapatinib

(A) Transition times are indicated for the best fit of M3 with 10 μM gefitinib (red) or lapatinib (green), representing the time for 50% of receptors to switch at least once to the other state. The K_ds for gefitinib binding to the active conformation and lapatinib binding to the inactive conformation were set at in vitro values, while the K_d for gefitinib binding the inactive conformation was fitted. Transition times are dependent on species concentrations; only a subset of possible transitions is shown (e.g., the gray arrow indicates that gefitinib can also bind non-phosphorylated receptors). A, active conformation; I, inactive conformation.

(B) ErbB1 phosphorylation following 10μM gefitinib or lapatinib exposure assuming progressive decreases in phosphorylation (k_1) and dephosphorylation (k_{-1}) rates from best fit values (dashed black). The k_1/k_{-1} ratio was held constant, with k_1 ranging from 209/min to 0.3/min and k_{-1} from 38/min to 0.06/min, and the predrug steady-state phosphorylation levels were rescaled to 40%.

(C) M3 prediction of the fraction of gefitinib-bound receptors in the active or inactive conformation (normalized by the total number of receptors) following addition of 10μM gefitinib at t = 10 min.

(D) HTM measurements of ErbB1-Y1173 phosphorylation in MCF-10A cells treated with EGF for 1 min and subsequently with gefitinib.

(E) M3 prediction and ErbB1-pY1173 measurements in H1666 cells of combination treatment with gefitinib and lapatinib (data for EGF treatment alone is dotted since M3 does not capture this behavior). The data shown are representative of experiments with various drug concentrations. See also Figure S6.

are still subject to rapid dephosphorylation and that lapatinib does not significantly bind to ErbB1 in the active conformation. We tested these assumptions by asking whether variant models could be fitted to the data (Figure 1D). Model M3-V1 assumes that only drug-bound receptors are dephosphorylated, and model M3-V2 assumes that gefitinib and lapatinib both bind only to the active conformation of ErbB1. When a multistart search was performed across a large range of values for all model parameters and fits to data were calculated, M3-V1 and M3-V2 were rejected with high confidence relative to the parental model M3 ($p < 10^{-10}$). Furthermore, if we allowed lapatinib to choose between the two conformations using model M3-V3, negligible binding was observed to the active conformation.

Two interesting M3 predictions with respect to ErbB1 phospho-dynamics were testable in cells. First, low-dose gefitinib should result in a state of chronic sub-maximal receptor activity. Consistent with this, we observed that addition of 0.5–1 μM gefitinib to MCF-1A or H1666 cells 1–2 min after EGF stimulation led to fractional ErbB1-Y1173 phosphorylation that was sustained for many hours (Figure 7D and Figure S6A). Under these conditions, ErbB1 was not detectably degraded and did not translocate to late endosomes as usual following EGF treatment (Figures S6B and S6C). Similar results were obtained when cells were pretreated with gefitinib for 1 hr before addition of EGF (Figure S6D). Thus, one consequence of rapid

ErbB1 cycling between unmodified and phospho-states in the presence of subsaturating gefitinib appears to be the generation of a pool of receptors whose level or rate of phosphorylation is insufficient to trigger normal adaptation or degradation. Moreover, the phenomenon occurs at drug concentrations approximating the maximum serum concentration in human patients (~0.5-1 μM) (Baselga et al., 2002).

A second model prediction is that gefitinib should interfere with the ability of low-dose lapatinib to promote complete ErbB1 dephosphorylation. Interference is predicted to be subtle but could be confirmed experimentally. When gefitinib and lapatinib were simultaneously added to EGF-stimulated cells, ErbB1 dephosphorylation occurred in two phases: receptors were first rapidly dephosphorylated as a consequence of gefitinib binding to receptor in the active conformation and then were slowly inhibited as a consequence of lapatinib inducing a switch to the inactive conformation (Figure 7E). The latter step is slower in the presence of both drugs than lapatinib alone, suggesting that gefitinib interferes with lapatinib action by holding some receptors in the active state.

DISCUSSION

Ligand binding activates RTKs, resulting in their phosphorylation on multiple tyrosine residues that serve as binding sites for cytosolic adaptor proteins. Association of adaptors (and other proteins) promotes assembly of large multiprotein complexes that initiate immediate-early signaling. In this paper we quantify rates of turnover on the phosphotyrosine sites of activated RTKs and investigate the consequences for signaling and receptor inhibition by drugs. Our approach combines mathematical modeling, clinical-grade drugs and time course data on five RTKs, their adaptors and downstream signaling proteins in four cell lines. We find that very rapid turnover of activating sites of phosphorylation is a common property of RTKs and the downstream kinases they control. The classical view holds that RTKs such as ErbB1 rapidly acquire kinase activity upon ligand binding and are inactivated over 30–90 min by a combination of dephosphorylation, internalization, degradation and negative feedback (Avraham and Yarden, 2011). However, ErbB1 can be rapidly dephosphorylated when kinase activity is acutely inhibited by drugs (Böhmer et al., 1995; Offterdinger et al., 2004), and inactivation of tyrosine phosphatases using pervanadate has long been known to cause receptor phosphorylation (Ruff et al., 1997). These data imply rapid phospho-turnover of ErbB1 and chronic negative regulation by tyrosine phosphatases. Our analysis agrees with and extends these observations. We find that the half-lives of phosphorylated tyrosine residues on ErbB receptors are ~10–30 s (and possibly much shorter) and thus that receptors cycle between phosphorylated and unphosphorylated states at least 100–1000 times over the course of a typical immediate-early response. Phosphates on downstream signaling kinases (typically on serine and threonine residues involved in activation) also exhibit rapid turnover.

Our studies address three questions left unresolved by earlier experiments: (1) is rapid ErbB1 dephosphorylation an artifact of drug binding, (2) is the pool of ErbB1 subject to rapid phospho-turnover the same pool active in signal transduction, and (3) is rapid phospho-turnover observed with other RTKs? Several lines of evidence argue that the phospho-turnover we observe is not simply an artifact of drug binding. First, when EGF-treated cells are exposed to the ErbB1-selective inhibitor gefitinib, rapid dephosphorylation occurs on many proteins that do not themselves bind drug, including other RTKs (e.g., ErbB2 and ErbB3), adaptor proteins (e.g., Shc) and downstream kinases (e.g., Akt, ERK and p38). It is highly improbable that changes in ErbB1 induced by drug binding could affect these other proteins, several of which do not interact with ErbB1 directly. Moreover, rapid dephosphorylation is observed following simple ligand washout and for a range of small molecules and antibody drugs that bind to ErbB1 in different ways. Finally, analysis of a computational model in which we assume rapid dephosphorylation to be restricted to drug-bound receptors is rejected with high probability based on a comparison to data.

The fact that ErbB1 inhibition results in rapid dephosphorylation of downstream signaling proteins and cessation of lamellipod extension (an immediate-early response to EGF) demonstrates that the pool of ErbB1 subject to rapid phospho-turnover is the pool active in signaling. Moreover, rapid phospho-turnover is not restricted to ErbB1 and the same phenomenon can be observed (or inferred) for EGF-activated ErbB2 and ErbB3, and for IGF1R and FGFR1. From these and other data we conclude that rapid phospho-turnover is a normal feature of RTK biology that occurs over a wide range of ligand concentrations in transformed and non-transformed cells. Fast cycling between phosphorylated and dephosphorylated states has also been observed for high affinity IgE receptors, which normally mediate inflammatory reactions including allergic responses (Mao and Metzger, 1997). We hypothesize that many receptor-mediated events at the plasma membrane exhibit high dynamicity, potentially allowing cells to respond rapidly to changes in the extracellular environment.

Consequences of Phospho-Turnover for Signal Transduction

Rapid turnover of tyrosine phosphates on RTKs implies rapid assembly and disassembly of signaling complexes, since binding of SH2 and PTB domains to tyrosine phosphates has been shown to protect modified residues from phosphatases (Brunati et al., 1998). This hypothesis is consistent with data on binding affinities and protein abundance. We measured a similar concentration of ErbB1 and the Shc1 p52 isoform in H1666 cells (see the Supplemental Experimental Procedures), and assuming a Shc1 affinity of ~150 nM (Jones et al., 2006), model M3 predicts that in the presence of saturating ligand ~15% of ErbB1 is Shc-bound with a $t_{1/2}$ ~2 s for the complex (a finding consistent with immunoprecipitation data). Short half-lives should result in shuttling of SH2 and PTB-containing adaptors among binding sites on the same or neighboring RTKs, a situation analogous to the shuttling of G protein subunits among seven transmembrane domain receptors (Linderman, 2009).

Shuttling of adaptor proteins among signaling complexes has significant implications for modeling "combinatorial complexity" (Hlavacek et al., 2003). Simple enumeration of all oligomeric, phospho and assembly states of ErbB1 suggests at least 10^7 biochemically distinct species (Schulze et al., 2005), but it is

extremely challenging to model such complexity. Moreover, since the number of states exceeds the number of receptors (10^4–10^6 molecules/cell) each state must have very low fractional occupancy, which is expected to result in large stochastic fluctuations. However, if assembly states interconvert on time scales that are rapid (seconds) relative to the time scales of immediate-early signaling (tens of minutes), RTKs can be modeled as having a time-averaged quasi-static state structure that involves considerably fewer states. Similar mathematical approximations have recently been described to model complex patterns of multi-site phosphorylation (Thomson and Gunawardena, 2009).

From our data, it follows that RTKs and cytosolic kinases such as Akt, ERK, and p38 are all antagonized by potent phosphatases. Theoretical studies suggest phosphatases to be among the most critical and least understood regulators of signal transduction (Heinrich et al., 2002). In the case of ErbB1, phosphatases appear to be active in multiple subcellular compartments including the plasma membrane. Biochemical fractionation and cloning experiments have identified multiple enzymes with the potential to antagonize ErbB1 kinase activity (Table S3) (Tiganis, 2002), some of which have been implicated in receptor activation by UV or free radicals (Xu et al., 2006). The connection between the rapid phospho-turnover we observe and net decline in receptor modification that occurs on a longer time scale during receptor adaptation remains to be elucidated: we measure equally rapid phospho-turnover of ErbB1 and ErbB2 in cells in which the natural half-life of phosphorylated receptors (in the absence of drug) varies between 12 and 90 min. Perhaps rapid phospho-turnover is involved in setting the sensitivity of RTK signaling, by loose analogy to the zero-order sensitivity observed with cycling enzymatic systems (Goldbeter and Koshland, 1981).

The turnover of upstream and downstream signaling molecules is not always tightly linked: we find that rapid receptor inactivation has a variable effect on the rate of dephosphorylation of a dozen downstream proteins across a panel of four cell lines. In the case of phospho-ERK for example, rapid decay is observed after ErbB1 inhibition in MCF-10A cells, but dephosphorylation is slower in H1666 cells. H1666 cells indeed contain active ERK-directed phosphatases, since pharmacological inhibition of the kinase for ERK (MEK) causes rapid ERK dephosphorylation. Instead, it seems that one or more proteins linking ERK to ErbB1 (e.g., Ras or Raf) have longer-lived active states in H1666 cells. It will be worth investigating this phenomenon in greater detail to see if it might play a role in oncogenic transformation.

Quantifying Phospho-Turnover Rates and Investigating Consequences for RTK Pharmacology

Rates of receptor phospho-turnover in cells are not directly observable using existing methods but they can be inferred by creating models of receptor biochemistry, calibrating the models to experimental data and subjecting model-based predictions to empirical tests. In this paper, we use a succession of models differing in complexity to reconcile the competing demands of identifiability (possible with simple models) and biochemical reality (which is complex). Rate constants estimated using different models vary in magnitude, with an increase in the number of assumed biochemical states generally resulting in faster rates (hence the ranges cited in Figure 1D). Since models M1–M3 are not particularly detailed in comparison to the actual biochemistry or even to models we and others have published previously (e.g., Blinov et al., 2006; Chen et al., 2009), our estimated rate constants represent lower bounds; it is probable that actual rates are higher.

The real value of kinetic modeling is not to derive rate constants but to understand the logic and dynamics of complex multi-step processes, in the current case the mechanisms of action of gefitinib and lapatinib, exemplars of two classes of small molecule ErbB1 kinase inhibitors. We have analyzed model M3 using a newly developed method of in silico labeling that makes it possible to estimate flux-based transition times between states in the face of parameter non-identifiability. Flux estimates are more tightly constrained than estimates of elementary rate constants, probably because they are computed from ratios of correlated parameters (Chen et al., 2009). In vitro, gefitinib binds rapidly and reversibly to ErbB1 in an active conformation (Yun et al., 2007) whereas lapatinib binds to an inactive conformation and acts as though it is irreversible (Wood et al., 2004). Experimentally we observe two significant differences between gefitinib and lapatinib in cells: ErbB1 dephosphorylation in the presence of gefitinib is rapid but incomplete at clinically accessible doses (<2 μM for cells with wild-type ErbB1) and results in chronic receptor activation. Lapatinib inhibits receptors >20-fold more slowly but it eventually results in complete inhibition even at low doses. Sustained receptor activation in the presence of gefitinib is a direct result of rapid phospho-turnover, competition from millimolar intracellular ATP and rapid reformation of active receptors. Indeed, model analysis suggests that competition from ATP is so significant in the mechanism of drug action, that complexes between inactive ErbB1 and gefitinib are 4-fold more abundant than between active ErbB1 and gefitinib (at 10 μM gefitinib), even though gefitinib binds ~150-fold more avidly to active ErbB1.

In the case of lapatinib, we hypothesize that slow inactivation of receptor is dominated not by the on-rate for binding to inactive ErbB1 as proposed previously (Wood et al., 2004), even though it is ~10^5 slower than for gefitinib, but instead by an active-to-inactive conformational transition that is one to two orders of magnitude slower again. M3 predicts that it takes ~20 min for half of all active receptors to switch to the inactive conformation, and that these receptors then bind drug in ~30 s (at 10 μM lapatinib). Once lapatinib is bound, switching back to the active conformation is very slow (>10 days), not simply because the rate constant for lapatinib unbinding is low, but because the concentration of inactive and drug-unbound ErbB1 is low. Thus, in the presence of gefitinib, the transition time from the inactive to active state is ~70 min, even though the rate constant for conformational switching for unbound ErbB1 is unaffected by drug. These observations make clear the value of computing fluxes that account for both rate constants and species concentrations.

Conclusions

The accuracy of our scheme for binding of gefitinib and lapatinib to ErbB1 necessarily depends on the validity of our models. This might appear to be a vulnerability peculiar to our computation-driven approach, but we have argued that a tight link between

assumptions and conclusions always exists in mechanistic studies (Spencer and Sorger, 2011). Mathematical modeling simply serves to make hidden assumptions explicit. Indeed, widely cited in vitro biochemical parameters for anti-ErbB drugs were calculated using arithmetic formalisms that also make strong assumptions about quasi-static states (Chen et al., 2010). We cannot prove that our models are uniquely correct or that we have fully accounted for experimental uncertainty and error, but computational models have the merit that they can be readily and transparently modified as new ideas emerge, allowing old and new hypotheses to be rigorously compared. Arguments in favor of the conclusions presented here include the following: (1) enzymatic and drug binding parameters estimated using models and cell-based data are largely consistent with in vitro measurements and those discrepancies that exist can be rationalized, (2) fundamental conclusions are not particularly sensitive to model topology, with three distinct formulations (M1–M3) all yielding similar conclusions about phospho-turnover, and (3) several variant models that explore alternative hypotheses can be rejected on the basis of comparison to data. The conclusions in this paper also have clear implications for drug development. They suggest that in the case of kinases with slow active-to-inactive transitions it is significantly more important to optimize binding to inactive than active conformations. When these transitions are more rapid or ATP is able to bind appreciably to both conformations, it should be possible to use modeling to compute tradeoffs involved in developing drugs that bind to various kinase states with differing affinities.

EXPERIMENTAL PROCEDURES

Cell Lines and Materials

H1666, MCF-10A, HeLa, and HepG2 cells were cultured using standard media and protocols. Recombinant human EGF, IGF1, and FGF1 were purchased from PeproTech, amphiregulin from R&D Systems, canertinib from WuXi PharmaTech, gefitinib and lapatinib from LC Laboratories, NVP-AEW541 from Cayman Chemical, PD173074 from Stemgent and PD0325901 from Selleck. Mouse mAb225 was a gift from J. Spangler and D. Wittrup. Pervanadate was prepared by mixing equal amounts of activated Na_3VO_4 and H_2O_2 (Sigma) in water 10 min before use. Biochemical assays were performed using standard protocols that are described in the Supplemental Experimental Procedures.

Mathematical Modeling

M1, M2, and M2-MC were formulated and analyzed within Mathematica as ordinary differential equations or as stochastic processes. The MATLAB toolbox PottersWheel (Maiwald and Timmer, 2008) was used to perform differential equation modeling of M3 and to apply Maximum-Likelihood parameter calibration based on experimental data. All models are described in detail in the Computational Procedures section of the Supplemental Experimental Procedures.

SUPPLEMENTAL INFORMATION

Supplemental Information includes Supplemental Experimental Procedures, six figures, three tables, and five model files and can be found with this article online at doi:10.1016/j.molcel.2011.07.014.

ACKNOWLEDGMENTS

We thank V. Becker, W. Chen, S. Spencer, P. Jasper, and M. Lazzara and the Nikon Imaging Center at Harvard Medical School for help with light microscopy. This work was supported by National Institutes of Health grants GM68762 and CA112967 to P.K.S and D.A.L. P.K.S. is a founder and P.K.S. and D.A.L. are consultants and scientific advisory board members for Merrimack Pharmaceuticals.

Received: August 19, 2010
Revised: May 7, 2011
Accepted: July 15, 2011
Published: September 1, 2011

REFERENCES

Amanchy, R., Kalume, D.E., Iwahori, A., Zhong, J., and Pandey, A. (2005). Phosphoproteome analysis of HeLa cells using stable isotope labeling with amino acids in cell culture (SILAC). J. Proteome Res. *4*, 1661–1671.

Avraham, R., and Yarden, Y. (2011). Feedback regulation of EGFR signalling: decision making by early and delayed loops. Nat. Rev. Mol. Cell Biol. *12*, 104–117.

Baselga, J., Rischin, D., Ranson, M., Calvert, H., Raymond, E., Kieback, D.G., Kaye, S.B., Gianni, L., Harris, A., Bjork, T., et al. (2002). Phase I safety, pharmacokinetic, and pharmacodynamic trial of ZD1839, a selective oral epidermal growth factor receptor tyrosine kinase inhibitor, in patients with five selected solid tumor types. J. Clin. Oncol. *20*, 4292–4302.

Baulida, J., Kraus, M.H., Alimandi, M., Di Fiore, P.P., and Carpenter, G. (1996). All ErbB receptors other than the epidermal growth factor receptor are endocytosis impaired. J. Biol. Chem. *271*, 5251–5257.

Blinov, M.L., Faeder, J.R., Goldstein, B., and Hlavacek, W.S. (2006). A network model of early events in epidermal growth factor receptor signaling that accounts for combinatorial complexity. Biosystems *83*, 136–151.

Böhmer, F.D., Böhmer, A., Obermeier, A., and Ullrich, A. (1995). Use of selective tyrosine kinase blockers to monitor growth factor receptor dephosphorylation in intact cells. Anal. Biochem. *228*, 267–273.

Brunati, A.M., Pinna, L.A., Bergantino, E., Ruzzene, M., Cirri, P., Ramponi, G., and Donella-Deana, A. (1998). Src homology-2 domains protect phosphotyrosyl residues against enzymatic dephosphorylation. Biochem. Biophys. Res. Commun. *243*, 700–705.

Chen, W.W., Schoeberl, B., Jasper, P.J., Niepel, M., Nielsen, U.B., Lauffenburger, D.A., and Sorger, P.K. (2009). Input-output behavior of ErbB signaling pathways as revealed by a mass action model trained against dynamic data. Mol. Syst. Biol. *5*, 239.

Chen, W.W., Niepel, M., and Sorger, P.K. (2010). Classic and contemporary approaches to modeling biochemical reactions. Genes Dev. *24*, 1861–1875.

Chung, I., Akita, R., Vandlen, R., Toomre, D., Schlessinger, J., and Mellman, I. (2010). Spatial control of EGF receptor activation by reversible dimerization on living cells. Nature *464*, 783–787.

Citri, A., and Yarden, Y. (2006). EGF-ERBB signalling: towards the systems level. Nat. Rev. Mol. Cell Biol. *7*, 505–516.

Goldbeter, A., and Koshland, D.E., Jr. (1981). An amplified sensitivity arising from covalent modification in biological systems. Proc. Natl. Acad. Sci. USA *78*, 6840–6844.

Haj, F.G., Verveer, P.J., Squire, A., Neel, B.G., and Bastiaens, P.I. (2002). Imaging sites of receptor dephosphorylation by PTP1B on the surface of the endoplasmic reticulum. Science *295*, 1708–1711.

Heinrich, R., Neel, B.G., and Rapoport, T.A. (2002). Mathematical models of protein kinase signal transduction. Mol. Cell *9*, 957–970.

Hirsch, D.S., Shen, Y., and Wu, W.J. (2006). Growth and motility inhibition of breast cancer cells by epidermal growth factor receptor degradation is correlated with inactivation of Cdc42. Cancer Res. *66*, 3523–3530.

Hlavacek, W.S., Faeder, J.R., Blinov, M.L., Perelson, A.S., and Goldstein, B. (2003). The complexity of complexes in signal transduction. Biotechnol. Bioeng. *84*, 783–794.

Holbro, T., and Hynes, N.E. (2004). ErbB receptors: directing key signaling networks throughout life. Annu. Rev. Pharmacol. Toxicol. *44*, 195–217.

Huyer, G., Liu, S., Kelly, J., Moffat, J., Payette, P., Kennedy, B., Tsaprailis, G., Gresser, M.J., and Ramachandran, C. (1997). Mechanism of inhibition of protein-tyrosine phosphatases by vanadate and pervanadate. J. Biol. Chem. *272*, 843–851.

Johnson, L.N. (2009). Protein kinase inhibitors: contributions from structure to clinical compounds. Q. Rev. Biophys. *42*, 1–40.

Jones, R.B., Gordus, A., Krall, J.A., and MacBeath, G. (2006). A quantitative protein interaction network for the ErbB receptors using protein microarrays. Nature *439*, 168–174.

Karaman, M.W., Herrgard, S., Treiber, D.K., Gallant, P., Atteridge, C.E., Campbell, B.T., Chan, K.W., Ciceri, P., Davis, M.I., Edeen, P.T., et al. (2008). A quantitative analysis of kinase inhibitor selectivity. Nat. Biotechnol. *26*, 127–132.

Kaushansky, A., Gordus, A., Chang, B., Rush, J., and MacBeath, G. (2008). A quantitative study of the recruitment potential of all intracellular tyrosine residues on EGFR, FGFR1 and IGF1R. Mol. Biosyst. *4*, 643–653.

Linderman, J.J. (2009). Modeling of G-protein-coupled receptor signaling pathways. J. Biol. Chem. *284*, 5427–5431.

Maiwald, T., and Timmer, J. (2008). Dynamical modeling and multi-experiment fitting with PottersWheel. Bioinformatics *24*, 2037–2043.

Mao, S.Y., and Metzger, H. (1997). Characterization of protein-tyrosine phosphatases that dephosphorylate the high affinity IgE receptor. J. Biol. Chem. *272*, 14067–14073.

Neelam, B., Richter, A., Chamberlin, S.G., Puddicombe, S.M., Wood, L., Murray, M.B., Nandagopal, K., Niyogi, S.K., and Davies, D.E. (1998). Structure-function studies of ligand-induced epidermal growth factor receptor dimerization. Biochemistry *37*, 4884–4891.

Nishimura, Y., Bereczky, B., and Ono, M. (2007). The EGFR inhibitor gefitinib suppresses ligand-stimulated endocytosis of EGFR via the early/late endocytic pathway in non-small cell lung cancer cell lines. Histochem. Cell Biol. *127*, 541–553.

Northrup, S.H., and Erickson, H.P. (1992). Kinetics of protein-protein association explained by Brownian dynamics computer simulation. Proc. Natl. Acad. Sci. USA *89*, 3338–3342.

Offterdinger, M., Georget, V., Girod, A., and Bastiaens, P.I. (2004). Imaging phosphorylation dynamics of the epidermal growth factor receptor. J. Biol. Chem. *279*, 36972–36981.

Paez, J.G., Jänne, P.A., Lee, J.C., Tracy, S., Greulich, H., Gabriel, S., Herman, P., Kaye, F.J., Lindeman, N., Boggon, T.J., et al. (2004). EGFR mutations in lung cancer: correlation with clinical response to gefitinib therapy. Science *304*, 1497–1500.

Pratilas, C.A., Hanrahan, A.J., Halilovic, E., Persaud, Y., Soh, J., Chitale, D., Shigematsu, H., Yamamoto, H., Sawai, A., Janakiraman, M., et al. (2008). Genetic predictors of MEK dependence in non-small cell lung cancer. Cancer Res. *68*, 9375–9383.

Qiu, C., Tarrant, M.K., Boronina, T., Longo, P.A., Kavran, J.M., Cole, R.N., Cole, P.A., and Leahy, D.J. (2009). In vitro enzymatic characterization of near full length EGFR in activated and inhibited states. Biochemistry *48*, 6624–6632.

Roepstorff, K., Grandal, M.V., Henriksen, L., Knudsen, S.L., Lerdrup, M., Grøvdal, L., Willumsen, B.M., and van Deurs, B. (2009). Differential effects of EGFR ligands on endocytic sorting of the receptor. Traffic *10*, 1115–1127.

Ruff, S.J., Chen, K., and Cohen, S. (1997). Peroxovanadate induces tyrosine phosphorylation of multiple signaling proteins in mouse liver and kidney. J. Biol. Chem. *272*, 1263–1267.

Schulze, W.X., Deng, L., and Mann, M. (2005). Phosphotyrosine interactome of the ErbB-receptor kinase family. Mol. Syst. Biol. *1*, 2005, 0008.

Segall, J.E., Tyerech, S., Boselli, L., Masseling, S., Helft, J., Chan, A., Jones, J., and Condeelis, J. (1996). EGF stimulates lamellipod extension in metastatic mammary adenocarcinoma cells by an actin-dependent mechanism. Clin. Exp. Metastasis *14*, 61–72.

Sorkin, A., and Goh, L.K. (2009). Endocytosis and intracellular trafficking of ErbBs. Exp. Cell Res. *315*, 683–696.

Spencer, S.L., and Sorger, P.K. (2011). Measuring and modeling apoptosis in single cells. Cell *144*, 926–939.

Thomson, M., and Gunawardena, J. (2009). Unlimited multistability in multisite phosphorylation systems. Nature *460*, 274–277.

Tiganis, T. (2002). Protein tyrosine phosphatases: dephosphorylating the epidermal growth factor receptor. IUBMB Life *53*, 3–14.

Wood, E.R., Truesdale, A.T., McDonald, O.B., Yuan, D., Hassell, A., Dickerson, S.H., Ellis, B., Pennisi, C., Horne, E., Lackey, K., et al. (2004). A unique structure for epidermal growth factor receptor bound to GW572016 (Lapatinib): relationships among protein conformation, inhibitor off-rate, and receptor activity in tumor cells. Cancer Res. *64*, 6652–6659.

Xu, Y., Shao, Y., Voorhees, J.J., and Fisher, G.J. (2006). Oxidative inhibition of receptor-type protein-tyrosine phosphatase kappa by ultraviolet irradiation activates epidermal growth factor receptor in human keratinocytes. J. Biol. Chem. *281*, 27389–27397.

Yarden, Y., and Sliwkowski, M.X. (2001). Untangling the ErbB signalling network. Nat. Rev. Mol. Cell Biol. *2*, 127–137.

Yun, C.H., Boggon, T.J., Li, Y., Woo, M.S., Greulich, H., Meyerson, M., and Eck, M.J. (2007). Structures of lung cancer-derived EGFR mutants and inhibitor complexes: mechanism of activation and insights into differential inhibitor sensitivity. Cancer Cell *11*, 217–227.

Yun, C.H., Mengwasser, K.E., Toms, A.V., Woo, M.S., Greulich, H., Wong, K.K., Meyerson, M., and Eck, M.J. (2008). The T790M mutation in EGFR kinase causes drug resistance by increasing the affinity for ATP. Proc. Natl. Acad. Sci. USA *105*, 2070–2075.

Zhang, X., Gureasko, J., Shen, K., Cole, P.A., and Kuriyan, J. (2006). An allosteric mechanism for activation of the kinase domain of epidermal growth factor receptor. Cell *125*, 1137–1149.